McGowan et al. EJNMMI Research (2018) 8:73
https://doi.org/10.1186/s13550-018-0430-4

EJNMMI Research

ORIGINAL RESEARCH Open Access

Whole tumor kinetics analysis of ^{18}F-fluoromisonidazole dynamic PET scans of non-small cell lung cancer patients, and correlations with perfusion CT blood flow

Daniel R. McGowan[1,2*], Michael Skwarski[1], Bartlomiej W. Papiez[3,4], Ruth E. Macpherson[5], Fergus V. Gleeson[1,5], Julia A. Schnabel[6], Geoff S. Higgins[1,7†] and John D. Fenwick[1,8†]

Abstract

Background: To determine the relative abilities of compartment models to describe time-courses of 18F-fluoromisonidazole (FMISO) tumor uptake in patients with advanced stage non-small cell lung cancer (NSCLC) imaged using dynamic positron emission tomography (dPET), and study correlations between values of the blood flow-related parameter K_1 obtained from fits of the models and an independent blood flow measure obtained from perfusion CT (pCT).

NSCLC patients had a 45-min dynamic FMISO PET/CT scan followed by two static PET/CT acquisitions at 2 and 4-h post-injection. Perfusion CT scanning was then performed consisting of a 45-s cine CT.

Reversible and irreversible two-, three- and four-tissue compartment models were fitted to 30 time-activity-curves (TACs) obtained for 15 whole tumor structures in 9 patients, each imaged twice. Descriptions of the TACs provided by the models were compared using the Akaike and Bayesian information criteria (AIC and BIC) and leave-one-out cross-validation. The precision with which fitted model parameters estimated ground-truth uptake kinetics was determined using statistical simulation techniques. Blood flow from pCT was correlated with K_1 from PET kinetic models in addition to FMISO uptake levels.

Results: An irreversible three-tissue compartment model provided the best description of whole tumor FMISO uptake time-courses according to AIC, BIC, and cross-validation scores totaled across the TACs. The simulation study indicated that this model also provided more precise estimates of FMISO uptake kinetics than other two- and three-tissue models. The K_1 values obtained from fits of the irreversible three-tissue model correlated strongly with independent blood flow measurements obtained from pCT (Pearson r coefficient = 0.81). The correlation from the irreversible three-tissue model ($r = 0.81$) was stronger than that from than K_1 values obtained from fits of a two-tissue compartment model ($r = 0.68$), or FMISO uptake levels in static images taken at time-points from tracer injection through to 4 h later (maximum at 2 min, $r = 0.70$).

Conclusions: Time-courses of whole tumor FMISO uptake by advanced stage NSCLC are described best by an irreversible three-tissue compartment model. The K_1 values obtained from fits of the irreversible three-tissue model correlated strongly with independent blood flow measurements obtained from perfusion CT ($r = 0.81$).

Keywords: FMISO, NSCLC, Dynamic PET, Kinetics analysis, Perfusion CT

* Correspondence: daniel.mcgowan@oncology.ox.ac.uk
†Geoff S. Higgins and John D. Fenwick contributed equally to this work.
[1]Department of Oncology, University of Oxford, Oxford OX3 7DQ, UK
[2]Radiation Physics and Protection, Oxford University Hospitals NHS Foundation Trust, Oxford, UK
Full list of author information is available at the end of the article

Springer Open

© The Author(s). 2018 **Open Access** This article is distributed under the terms of the Creative Commons Attribution 4.0 International License (http://creativecommons.org/licenses/by/4.0/), which permits unrestricted use, distribution, and reproduction in any medium, provided you give appropriate credit to the original author(s) and the source, provide a link to the Creative Commons license, and indicate if changes were made.

Background

The radiotracer ^{18}F-fluoromisonidazole (FMISO) diffuses passively into cells, where it is reduced and irreversibly bound in hypoxic environments. Thus, positron emission tomography (PET) imaging of FMISO uptake can be used to localize hypoxic tumor subvolumes [1–3]. The degree of hypoxia can be estimated either from uptake levels seen in single FMISO images collected 2–4 h after tracer injection [4], or from analysis of the kinetics of FMISO uptake in dynamic sequences of PET images (dPET). The kinetic analysis provides fitted values of model rate-constants related to blood flow and FMISO transport and intracellular binding and can be performed at the whole tumor level or voxel-by-voxel. For head-and-neck cancers, it has generated indices that correlate with radiotherapy (RT) outcomes [5].

Blood flow is often imaged using a perfusion CT (pCT) technique first proposed in 1980, in which iodine containing contrast is injected as a bolus through a venous cannula, and its passage through the patient is dynamically imaged and kinetically analyzed on the assumption that iodine concentrations within tissues are linearly proportional to changes in measured CT attenuation [6]. Blood flow measures obtained from pCT have been found to correlate with perfusion measurements obtained from dPET imaging of ^{15}O-water uptake [7], which in turn were correlated with kinetics indices obtained from compartment modeling of the first 2 min of ^{18}F-fluorodeoxyglucose (FDG) dPET scans [8].

In this study, we investigate which of several compartment models best describes PET-imaged time-courses of FMISO uptake in whole NSCLC tumors, and we identify the model whose fits to the time-course data provide the most precise estimates of tracer kinetics rate-constants according to statistical simulations. Correlations are determined between perfusion measures obtained directly from the PET FMISO kinetics model fits and independently from pCT.

Methods

PET and pCT image acquisition and processing

In a pre-clinical study, the investigational drug buparlisib (Novartis) reduced tumor hypoxia in vivo [9]. A clinical trial (BKM120) completed in Oxford (NCT02128724) has the primary aim of determining the maximum tolerated dose of buparlisib in non-small cell lung cancer (NSCLC) patients treated palliatively using radiotherapy, and the secondary goal of validating the pre-clinical results in these patients, who are imaged using FMISO PET at baseline and 7 days after administration of buparlisib without any other intervention. The study has been approved by the local ethics committee and signed informed consent obtained from all patients.

Patients were imaged supine with their arms by their side using a GE Discovery 690 PET/CT scanner (GE Healthcare). They were injected with 370 MBq FMISO 30 s into PET imaging, which continued for 45 min and resumed for 10 min intervals at 2 and 4-h post-injection. Prior to each PET acquisition, a CT scan was performed for localization and PET attenuation correction. PET images were reconstructed using a time-of-flight ordered subset expectation maximization algorithm (VPFX, GE Healthcare). The first 45 min of data were binned into two parallel time sequences, S1 (1 s × 30 s, 12 s × 5 s, 6 s × 10 s, 5 s × 30 s, 10 s × 60 s, 6 s × 300 s) and S2 (1 s × 30 s, 60 s × 1 s, 12 s × 10 s, 3 s × 30 s, 10 s × 60 s, 6 s × 300 s), and reconstructed as images on a matrix of 5.5 mm^3 × 5.5 mm^3 × 3.3 mm^3 voxels. Data collected during the two later 10-min intervals were processed as single frames [10].

pCT scanning was performed immediately after PET/CT imaging concluded at 4-h post-injection of FMISO, with patients set up in the same position on the same PET/CT scanner. Initially a pre-contrast CT scan (helical mode, 120 kV, smart mA, 32 noise index) was carried out to determine the region over which the pCT data would be collected. Then pCT scanning commenced (120 kV, 60 mA), collecting one 3D image in each of 45 consecutive seconds, over an axial length of 40 mm corresponding to the CT detector width. During pCT scanning 70 mL contrast (Omnipaque 300) was injected at 5 mL/s, followed by 25 mL water at 5 mL/s, with patients instructed to hold their breath at inspiration for as long as possible, breathing out very slowly if necessary.

For each patient, the primary tumor, involved nodes, and metastases were outlined on the PET/CT images by an experienced radiologist, and a blood region was defined within the central part of the descending aorta on five or more consecutive PET axial slices [11]. These were outlined on the CT images with the patient's prior contrast-enhanced CT imaging used to assist in determining tumor regions. Time-activity curves (TACs) representing time-courses of mean FMISO tracer activity concentrations within each tumor volume-of-interest (VOI) and the blood region were obtained from PET sequences S1 and S2 respectively. Activity data from the 10-min frames collected at 2 and 4 h post-injection were appended to the TACs. A total of 30 whole-volume tumor FMISO uptake TACs, obtained for 15 volumes-of-interest (9 primary tumors, 5 involved nodes, and 1 metastasis) in 9 patients, each imaged twice were studied (Table 1). Using a standard tumor to blood ratio of 1.4 (on the static images four hours post-injection), all of these whole tumor volumes had a number of voxels within them which could be considered to be hypoxic [4]. No direct oxygen measurements of the tumors were made in this trial.

Using Hermes Hybrid Viewer software (Hermes Medical Solutions AB, Sweden), the CT images obtained at PET/CT were rigidly registered with the CT images collected just

Table 1 Details of the 30 whole tumor TACs analyzed

Patient	VOIs and TAC reference numbers in images taken pre/post drug administration
1	Primary (1/2)
2	Primary (3/4), metastasis (5/6)
3	Primary (7/8)
4	Primary (9/10)
5	Primary (11/12)
6	Primary (13/14), node (15/16)
7	Primary (17/18), node (19/20)
8	Primary (21/22), node 1 (23/24), node 2 (25/26), node 3 (27/28)
9	Primary (29/30)

before pCT, allowing outlines of the primary tumors defined on the PET/CT to be transferred to the pCT scans. An example of a FMISO PET/CT image 4 h post-injection is shown in Fig. 1.

PET kinetics analysis and model fitting

Several methods have been used to analyze dPET data, the most common being compartment modeling [12]. Figure 2 illustrates reversible two-, three-, and four-tissue linear compartment models which we have fitted to time-courses of tumor tracer uptake [13–15]. FMISO binding is generally considered irreversible, and therefore, alongside reversible models, we have also studied irreversible models in which the rate-constant describing movement of bound to unbound tracer is set to zero. The compartment model developed by Casciari et al. [2] attempts to reflect the chemical processes that occur for FMISO uptake; however, this model has many fitting parameters, and so in this work, simpler compartment models have been investigated. We denote by xCyK a model comprising a linear chain of x-tissue compartments (excluding blood-borne tracer) and y rate-constants, and in order to associate rate-constants with particular models, we add the subscript xC to the names of rate-constants, except for those of the three-tissue compartment model.

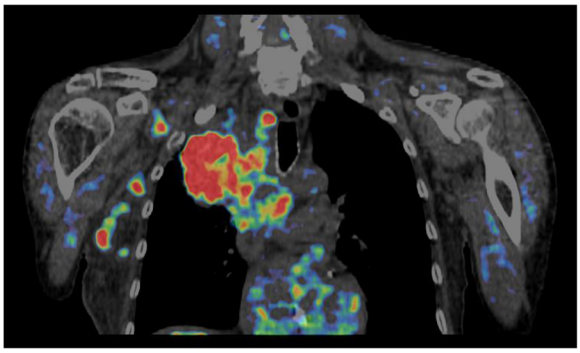

Fig. 1 An example coronal FMISO PET image fused with the corresponding CT displayed on a tumor to blood ratio (TBR) color scale. Red regions depict a TBR > 1.4 indicating hypoxia, and no visible PET depicts a TBR < 1, indicating normoxia [4]

Kinetics analysis was carried out using the PMOD system (PMOD Technologies) as described by McGowan et al. [10] In brief, an image-derived FMISO input function [16, 17] was obtained from the blood region outlined within the descending aorta, and a compartment model was fitted to the tumor TAC and input function data, generating fitted values of model rate-constants. Fitting was carried out by minimizing the weighted sum of squares between modeled and measured tumor uptake, using the Levenberg–Marquardt algorithm with weighting function

$$w_i = \Delta t_i \ \exp(-\lambda t_i)/C_{PET}(t_i) \tag{1}$$

where t_i and Δt_i are the mid-time post-injection and duration of the ith of T frames, λ is the decay constant for ^{18}F, and C_{PET} the measured PET activity concentration at time t_i [15, 17].

Model fitting was initiated from 100 randomly generated sets of starting values (suitably constrained), to attempt to reach global rather than local best fits [18]. Flux-constants were calculated from irreversible two-tissue compartment model (2C3K) fits as

$$k_{flux-2C} = \frac{K_{1-2C}\, k_{3-2C}}{k_{2-2C} + k_{3-2C}} \tag{2}$$

and from irreversible three-tissue (3C5K) compartment model fits as

$$k_{flux} = \frac{K_1 k_3 k_5}{k_2 k_4 + k_2 k_5 + k_3 k_5} \tag{3}$$

Assessment of PET kinetic model fits

The Wald–Wolfowitz runs-test was used to determine the adequacy of descriptions of FMISO uptake TACs provided by compartment model fits [19, 20]. To further assess the relative abilities of the different models to describe the data, we used the Akaike information criterion (AIC) [21] corrected for small sample size [22], the Bayesian information criterion (BIC) [22], and leave-one-out cross-validation [23]. The cross-validation approach proceeded by fitting each model to the complete dataset minus one point, calculating the differences between the value of the omitted data-point and values predicted by the models, repeating this process sequentially T times leaving out a different data-point each time, and finally calculating the mean of the squared error of prediction (MSEP) for each model, the model with the lowest MSEP being considered best. These model selection methods use slightly different criteria to determine the model that best describes the data (all penalizing highly

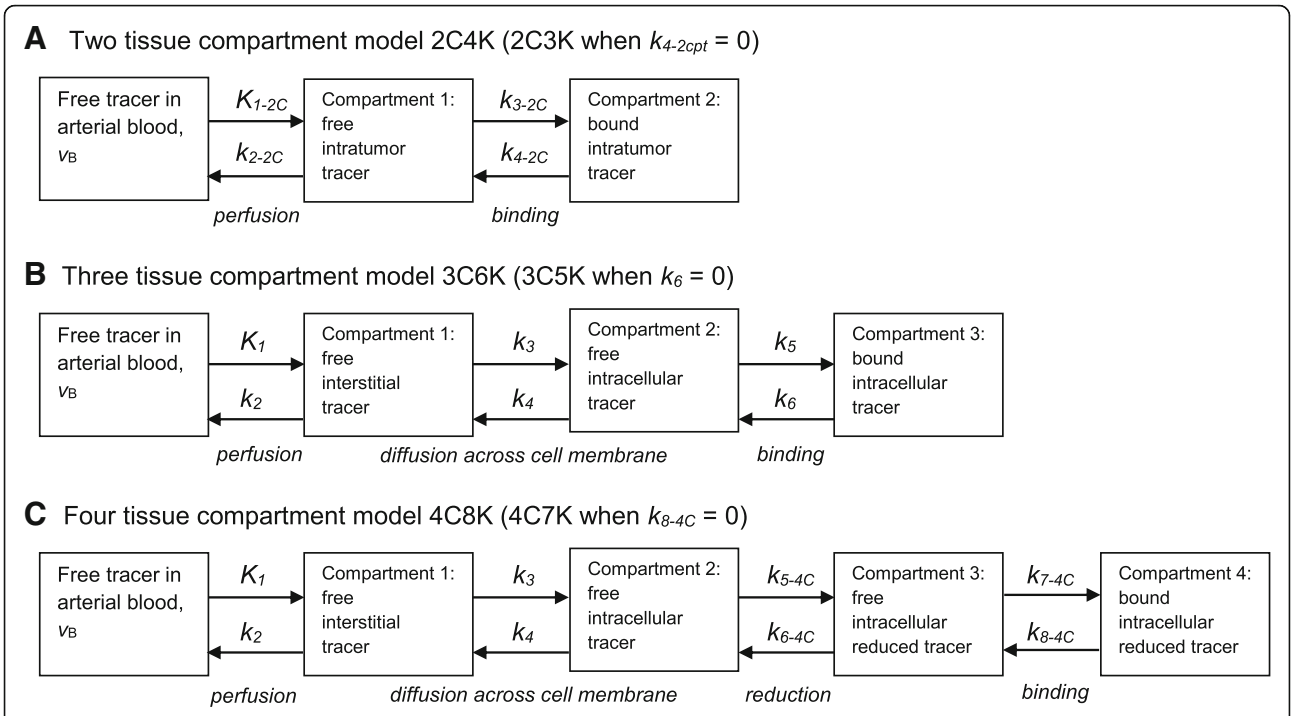

Fig. 2 **a** Two-, **b** three-, and **c** four-tissue compartment models used to analyze the dynamic PET data. Flow rates from one compartment to another are defined by rate-constants (*k* values), tracer concentrations and compartment volumes [12]. The fraction of the tumor volume occupied by blood is denoted in each model as v_B

parameterised models which are likely to over fit the data), for completeness all have been included in this work.

A statistical simulation procedure was used to assess which model produced the most accurate and precise rate-constant estimates [10]. For this analysis, we used 3C5K and 3C6K model fits to the 30 measured whole tumor TACs to create noise-free "ground-truth" TACs binned into the same frame-lengths as the original data, and the parameter values of these fits were taken as ground-truth rate-constants. For each of the resulting 60 ground-truth TACs, 1000 noisy TACs were simulated by adding normally distributed random variables to the activity concentrations of the individual time-frames, the variances of the noise differing between frames according to the inverse of Eq. (1) and scaled to match noise-levels seen on the measured whole tumor TACs [10, 15, 24–26]. The average whole tumor scaling factor with the weighting factor used here was 0.6 ± 0.3 (one standard deviation). The simulated TACs were then fitted using the 2C3K, 2C4K, 3C5K, and 3C6K models.

The simulated noise introduces random uncertainties and systematic error (bias) into fitted parameter values, adding to any underlying bias that results from mismatches between the fitted models and the ground-truth models used to generate the simulated TACs. As described by McGowan et al. [10], for each of the 30 ground-truth TACs associated with each ground-truth model, individual biases in parameter values were determined from fits to the 1000 noise realizations, and then these bias estimates were combined to calculate the overall mean bias (*MB*) and variance of bias values (σ_B^2) across the ground-truth TACs. The mean variance (σ_P^2) was calculated for each parameter as the average of the parameter variances obtained for each of the 30 ground-truth TACs. Then, the σ_B and σ_P terms were combined to generate a total uncertainty, σ_T, given by

$$\sigma_T = \left(\sigma_B^2 + \sigma_P^2\right)^{1/2} \tag{4}$$

For some fitted models, certain individual rate-constants are not uniquely related to any single ground-truth model parameter: for example, the processes described by the $K_{1\text{–}2C}$ parameter of two-compartment models are split between rate-constants K_1 and k_3 in three-compartment models. For such rate-constants, therefore, only the σ_P values were calculated.

Perfusion CT analysis and comparison with PET kinetic modeling

The small size of pCT image voxels (0.7 mm × 0.7 mm × 50 mm) makes parametric images of perfusion susceptible to movement [27], which can easily occur as it is difficult for patients to hold their breath for the full duration of pCT scanning. We therefore used a non-rigid image

registration algorithm to pre-process the pCT data. The algorithm was based on the diffeomorphic demons approach, modified by use of normalized gradient fields (NGF) to handle intensity changes caused by contrast uptake. The registration algorithm uses a multi-resolution framework with three levels (128 × 128 × 8, 256 × 256 × 8, 512 × 512 × 8), the final spacing being equal to the original voxel spacing. The maximum number of iterations for each level was 25, and the standard deviation of the Gaussian smoothing kernel was 2.8 mm, 1.4 mm, and 0.7 mm at the different resolution levels. Further details have been provided by Papiez et al [27].

The motion-corrected pCT data was then processed voxel-by-voxel using the commercial GE Perfusion 4D software (GE Healthcare, Milwaukee, USA). Voxel-by-voxel tumor blood flow information was obtained by fitting the Adiabatic Approximation to the Tissue Homogeneity (AATH) model [28] to the pCT TACs of each voxel, which describe the variation of voxel X-ray attenuation coefficient with time. Similarly to the compartment models used in the PET kinetics analysis, the AATH model describes the time-course of attenuation, and thus of iodine uptake, as the convolution of an iodine input function, obtained from a VOI drawn in the center of the descending aorta, with a residue function containing fittable parameters. A schematic of the AATH model is shown in Fig. 3: unlike the PET models, blood flowing through the tumor is considered to have a finite transit time, with contrast exchanged between intra and extravascular spaces only at the venous outlet.

Voxel-by-voxel values of blood flow, *BF*, were taken from the resulting parametric images and averaged over tumor volumes. Then, the averaged *BF* values for each tumor volume were compared to measures obtained from PET kinetics analysis. When the whole tumor volume exceeded the 4-cm axial length of the pCT scans, as shown in Fig. 4, the PET kinetic analysis was repeated just for the tumor subvolume lying within the pCT field

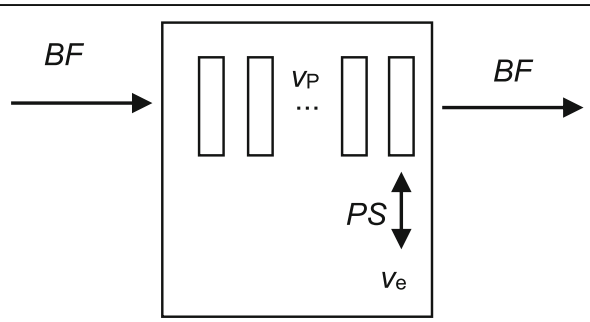

Fig. 3 Schematic of the AATH model used to analyze the perfusion CT data: *BF* is the blood flow through the tumor, v_P the intravascular plasma volume fraction, v_e the extracellular extravascular space, and *PS* the permeability surface area product which defines the exchange rate between plasma and the extravascular extracellular space

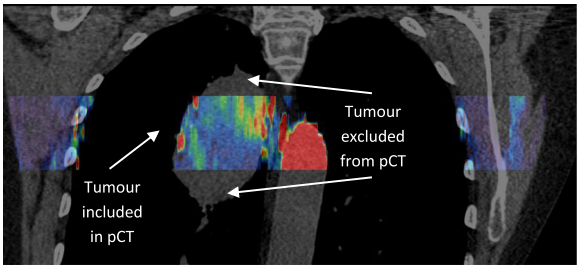

Fig. 4 A coronal slice taken from one patient; the section in color indicates the volume over which the pCT was performed, while the underlying greyscale CT is from the pre-contrast CT

of view, allowing results obtained from pCT perfusion and PET kinetics analyses to be meaningfully compared.

The K_1 rate-constant obtained from PET kinetic modeling is conceptually linked to *BF* via

$$K_1 = BF \times E \tag{5}$$

in which the extraction fraction *E* for a cylindrical capillary is given by [29, 30]

$$E = 1 - \exp(-PS/BF) \tag{6}$$

where *P* is capillary permeability, *S* the surface area per unit volume, and *PS* the permeability surface area product. For highly permeable tracers such as FMISO [31], *PS* is much greater than *BF* and the extraction fraction is close to 1. Consequently, *BF* measurements obtained from pCT scans should be approximately equal to K_1 derived from FMISO PET kinetic modeling. We have therefore determined the Pearson *r* coefficients of correlation between pCT tumor mean *BF* values and K_1 values obtained from 2C3K and 3C5K compartment model fits to the dPET data. Correlations were also evaluated between *BF* values and static FMISO uptakes at each time-point in the dynamic series of images, and between *BF* and the average FMISO uptakes over the first 2 min post-injection.

Results

Quality of compartment model fits to FMISO TACs

The numbers of whole tumor FMISO TACs for which fits of each compartment model passed the runs-test are listed in Table 2, together with total AIC, BIC, and MSEP scores for the different models summed over all TACs, and the numbers of TACs for which each model achieved the lowest scores. Runs-test results are presented individually for each whole tumor TAC in Additional file 1: Table S1 with corresponding AIC, BIC, and MSEP scores detailed in Additional file 2: Table S2.

The three- and four-tissue models passed the runs-test for 83–100% of whole tumor TACs, whereas two-tissue model fits passed for only 0–20% [32]. Summed AIC,

Table 2 Summary of runs-test results and totaled AIC, BIC, and MSEP scores for compartment model fits to all 30 whole tumor FMISO TACs. Lowest totaled AIC, BIC, and MSEP scores are underlined, indicating the best model according to those measures

Model	2C3K	2C4K	3C5K	3C6K	4C7K	4C8K
Runs-test passes from fits to all 30 TACs						
Runs	0	6	25	26	30	30
Information criteria and cross-validation scores summed for all TACs						
AIC	13,970	8600	1544	1554	1557	1644
BIC	14,174	8836	1813	1840	1850	1945
MSEP	219	131	24.6	26.9	24.8	27.9
Numbers of TACs for which each model has the lowest scores						
AIC	0	0	21	3	6	0
BIC	0	0	22	3	5	0
MSEP	0	0	24	3	3	0

BIC, and MSEP scores were much lower for three- and four-tissue models than for two-tissue models, which lacked the flexibility to describe the data well. Fits of the 2C3K, 2C4K, and 3C5K models to two example TACs (4 and 24) are plotted in Fig. 5.

The irreversible three-tissue model, 3C5K, achieved the lowest AIC, BIC, and MSEP scores totaled over all tumor TACs, and the lowest scores for most (21–24) individual TACs. Individual scores were generally a little higher for the 3C6K, 4C7K, and 4C8K models, their additional complexity usually being unnecessary to describe the TAC data.

Table 3 lists estimates of parameter accuracy and precision obtained from the statistical simulations, which used fits of the 3C5K and 3C6K models to measured FMISO TACs to represent the ground-truth, the 3C5K model offering the best description of the TACs according to the AIC, BIC, and MSEP measures. Parameter values obtained from fits of the 2C4K model to simulated noisy TACs had large mean biases and total uncertainties, irrespective of which three-tissue ground-truth model was used. Mean biases and uncertainties of fitted 2C3K model parameters were not so large as for 2C4K, but were still considerably larger than those estimated for three-compartment models.

For parameters v_B, K_1, k_2, k_3, and k_4, mean biases and total uncertainties were similar for 3C5K and 3C6K model fits, regardless of which three-tissue model was

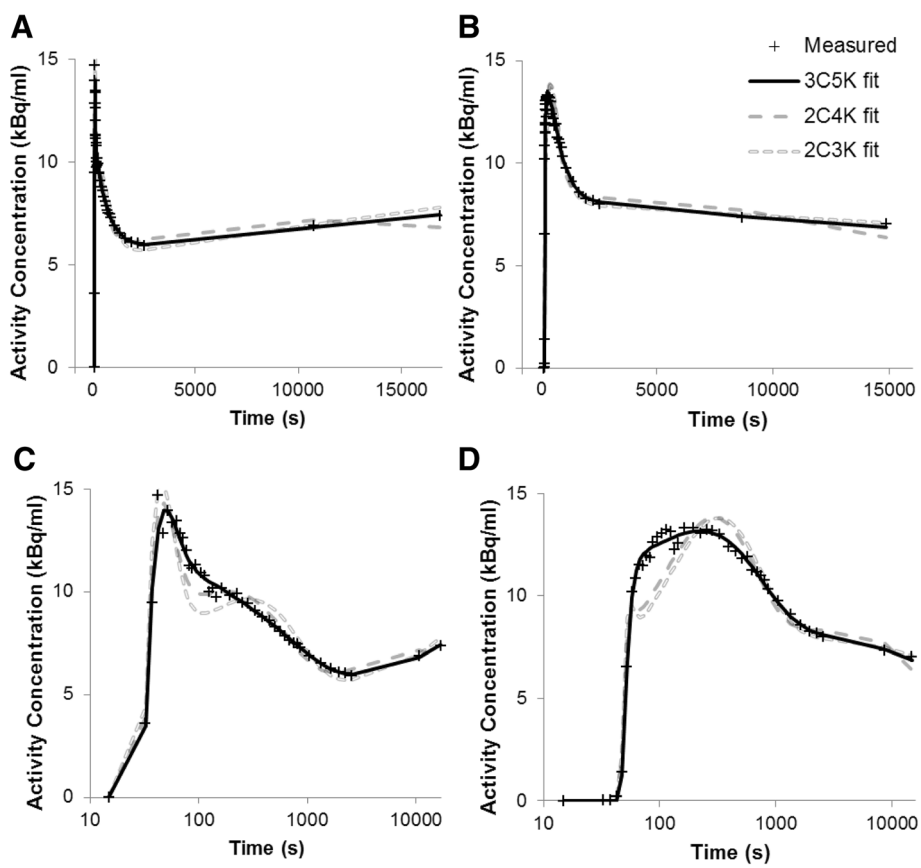

Fig. 5 Fits of the 2C3K, 2C4K, and 3C5K models to FMISO TACs 4 (plots **a** and **c**) and 24 (**b** and **d**). Time post-injection is plotted on linear (**a**/**b**) and logarithmic (**c**/**d**) scales to enable the early part of the TAC and modeled TAC to be visualized

Table 3 Estimates of the accuracy and precision of parameter values obtained from fits of the 2C3K, 2C4K, 3C5K, and 3C6K models to whole tumor TACs simulated by adding whole tumor-level noise to the ground-truth, represented as 3C5K and 3C6K model fits to real TACs. Values of MB, σ_B, σ_P and σ_T are shown for fitted parameters as percentages of the mean values of directly related ground-truth parameters in the 3C5K or 3C6K models. When no directly related parameter exists, σ_P is listed alone as a percentage of the mean fitted parameter value

Model fitted	Fitted model parameters							
Ground-truth 3C5K model								
2C3K	v_{B-2C}	K_{1-2C}	k_{2-2C}			k_{3-2C}		$k_{flux-2C}$
MB (%)	47	–	–			−40		25
σ_B (%)	24	–	–			23		11
σ_P (%)	14	30	36			12		13
σ_T (%)	27	–	–			26		17
2C4K	v_{B-2C}	K_{1-2C}	k_{2-2C}			k_{3-2C}	k_{4-2C}	$k_{flux-2C}$
MB (%)	25	–	–			565	–	1014
σ_B (%)	20	–	–			700	–	1049
σ_P (%)	9	7	13			73	45	47
σ_T (%)	22	–	–			704	–	1050
3C5K	v_B	K_1	k_2	k_3	k_4	k_5		k_{flux}
MB (%)	0	− 1	0	1	0	0		0
σ_B (%)	4	1	2	4	3	1		0
σ_P (%)	10	5	10	20	11	10		6
σ_T (%)	10	5	10	20	12	10		6
3C6K	v_B	K_1	k_2	k_3	k_4	k_5	k_6	k_{flux}
MB (%)	0	0	1	5	3	13	–	13
σ_B (%)	4	1	2	7	5	17	–	16
σ_P (%)	10	5	9	22	13	34	384	31
σ_T (%)	11	5	9	23	14	38	–	35
Ground-truth 3C6K model								
2C3K	v_{B-2C}	K_{1-2C}	k_{2-2C}			k_{3-2C}		$k_{flux-2C}$
MB (%)	48	–	–			− 51		4
σ_B (%)	24	–	–			49		33
σ_P (%)	13	36	42			11		10
σ_T (%)	27	–	–			50		35
2C4K	v_{B-2C}	K_{1-2C}	k_{2-2C}			k_{3-2C}	k_{4-2C}	$k_{flux-2C}$
MB (%)	25	–	–			510	3173	914
σ_B (%)	20	–	–			748	3768	1122
σ_P (%)	11	16	36			65	44	40
σ_T (%)	23	–	–			751	3768	1123
3C5K	v_B	K_1	k_2	k_3	k_4	k_5		k_{flux}
MB (%)	0	− 1	− 2	− 5	− 5	− 18		− 11
σ_B (%)	3	1	2	7	5	21		18
σ_P (%)	10	5	10	21	11	10		8
σ_T (%)	10	5	10	22	12	23		19
3C6K	v_B	K_1	k_2	k_3	k_4	k_5	k_6	k_{flux}
MB (%)	− 1	0	1	4	3	8	86	6
σ_B (%)	3	1	2	5	4	9	131	8
σ_P (%)	10	5	9	21	13	27	164	22
σ_T (%)	10	5	9	21	13	29	210	24

used to represent the ground-truth. For the k_5 and k_{flux} parameters, however, mean biases and total uncertainties were notably lower for 3C5K than for 3C6K model fits when the ground-truth was represented by the 3C5K model. Total uncertainties on 3C5K fits remained less than those on 3C6K fits even when the 3C6K model was used to represent the ground-truth, although in this circumstance 3C5K fit parameters had slightly higher mean biases than 3C6K fits.

Overall, the 3C5K model provided the most precise estimates of FMISO uptake kinetics according to statistical simulations, and the model's accuracy was only surpassed by 3C6K when this reversible model was also considered to represent the ground-truth, despite the known irreversibility of FMISO binding.

Correlations between K_1 and BF parameters obtained from FMISO dPET and pCT

Tumor K_1 values obtained from fits of the 3C5K and 2C3K models to the FMISO dPET data are plotted in Fig. 6 against BF values independently obtained from pCT analysis. The 3C5K-based K_1 values were strongly correlated with BF (Pearson r coefficient = 0.81), whereas 2C3K-based K_1 values were less strongly correlated ($r = 0.68$). Pearson r coefficients of correlation between BF and static FMISO tumor uptake in frames collected at different times are plotted in Fig. 7, the maximum correlation ($r = 0.70$) being obtained at 2-min post-injection.

Discussion

Whole tumor FMISO TACs obtained from dPET scans of advanced stage NSCLC patients were described better by an irreversible three-tissue compartment model, 3C5K, than by other compartment models we studied, according to information criterion and cross-validation scores, and statistical simulations. Total information criterion and cross-validation scores were much worse for simpler two-tissue compartment models and slightly worse for the reversible three-tissue model, 3C6K, and for four-tissue models whose additional complexity was unnecessary. In statistical simulation studies, total uncertainties calculated for fitted 3C5K model parameter values were consistently lower than those found for two-tissue compartment model fits, and a little lower than for 3C6K fits, even when the 3C6K model was used to represent the ground-truth.

For five of the measured whole tumor TACs, the 3C5K model fits did not pass a runs-test whereas the four-tissue compartment model fits did. For these particular TACs, we therefore carried out further statistical simulations, using 3C5K and 4C7K models as ground-truth. Even for these specific cases, fits of the 3C5K model provided more precise estimates of ground-truth kinetics values than did 4C7K fits, regardless of the ground-truth model used in the simulations.

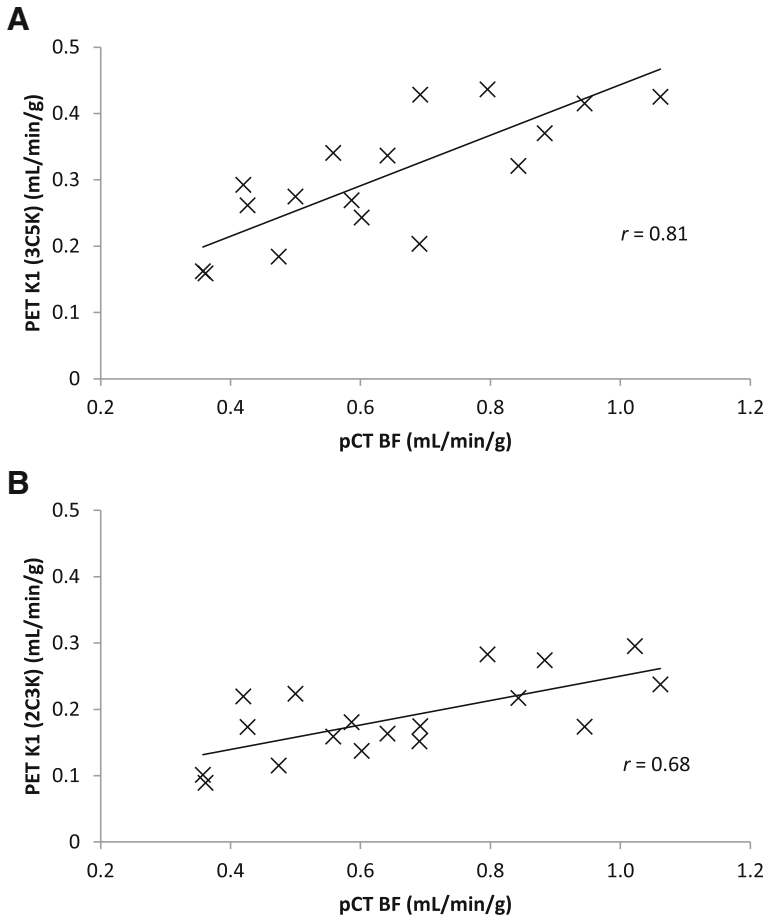

Fig. 6 K_1 values obtained from (**a**) 3C5K and (**b**) 2C3K compartment model fits to FMISO dPET data, plotted against *BF* values determined from pCT scans

A strong correlation ($r = 0.81$) was found between the K_1 parameter values of the 3C5K model fits to the FMISO TACs and *BF* values independently obtained from pCT. The K_1 values obtained from 2C3K model fits correlated less strongly (albeit not significantly less strongly) with *BF* ($r = 0.68$), lending weight to the results indicating that the 3C5K model describes whole tumor FMISO kinetics better than 2C3K. The K_1 values obtained from 3C5K model fits were also more strongly correlated with *BF* than were whole tumor FMISO

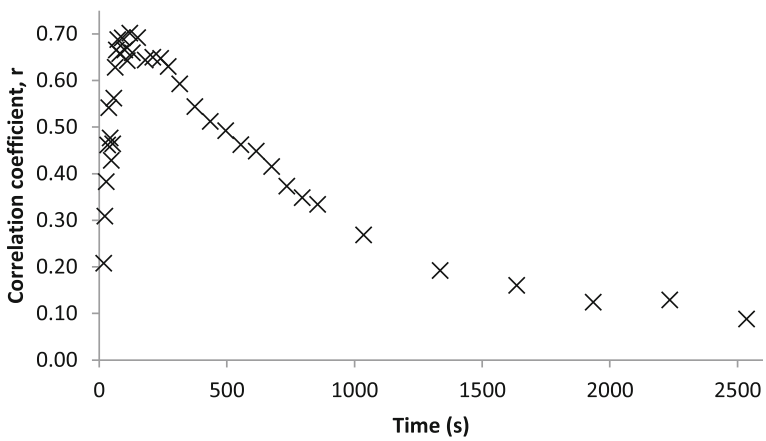

Fig. 7 Pearson *r* coefficients of correlation between *BF* values and FMISO uptake at a range of times post-injection

uptake values at times ranging from tracer injection to 4 h later (maximum correlation $r = 0.70$).

FMISO dPET imaging is used to measure hypoxia, and since hypoxia is related to perfusion, pCT perfusion scans are sometimes collected as well. Since *BF* is strongly correlated with the K_1 values obtained from 3C5K model fits to FMISO dPET data, blood flow could potentially be estimated directly from the K_1 values obtained from the FMISO images, rather than from pCT, thus saving time, money and the pCT radiation dose, and generating *BF* data over the 15 cm axial width of modern PET scanner fields-of-view, rather than 4-cm axial width typical of CT scanners used in cine-mode. Blood flow could also be estimated from FDG dPET data if available (not a hypoxia tracer), since *BF* values obtained from ^{15}O-labeled water dPET studies have previously been shown to strongly correlate with parameter values obtained from model fits to the first 2 min of FDG dPET scans ($r = 0.86$) [33].

The gold-standard method for determining input functions is direct arterial line sampling. However, we have used image-derived input functions (IDIFs) calculated from mean tracer activity concentrations within volumes drawn in the descending aorta, both for patient comfort and safety, and because good agreement has been demonstrated between directly sampled input functions and IDIFs obtained from the descending aorta [11].

In this study, we have assessed the performance of PET kinetic models in terms of information criteria scores, cross-validation measures, statistical simulations, and strengths of correlations with an independent measure of perfusion. The imaging protocol used in this work is demanding, as we are currently investigating whether shorter protocols can provide adequate rate-constant estimates. In a recently opened study (Atovaquone as Tumor HypOxia Modifier, NCT02628080), surgically treated NSCLC patients are being imaged using dynamic FMISO PET prior to tumor excision, allowing us to compare FMISO images and parametric maps directly with maps of histopathology obtained from excised tumor slices.

Conclusions

Time-courses of whole tumor FMISO uptake in patients with advanced stage NSCLC were described better by an irreversible three-tissue compartment model, 3C5K, than by other two-, three-, or four-tissue compartment models investigated. Fits of this model also provided the most precise estimates of FMISO uptake kinetics according to simulation studies. Further evidence for the utility of the 3C5K model was provided by the observation of a strong correlation ($r = 0.81$) between fitted values of its K_1 parameter and blood flow values obtained independently from perfusion CT imaging, a stronger correlation than that between blood flow and K_1 values obtained from 2C3K model fits, or between blood flow and tumor FMISO uptake in static scans taken at a range of times from immediately post-injection to 4 h later.

Additional files

Additional file 1: Table S1. TAC-by-TAC Wald-Wolfowitz runs-test results for fits of the different models (ticks indicate runs-test passes) (DOCX 38 kb)

Additional file 2: Table S2. Individual AIC, BIC and MSEP scores for fits of the various models to each TAC. The lowest AIC, BIC, and MSEP scores have been underlined for each TAC, indicating the best model according to that measure (DOCX 46 kb)

Abbreviations

2C3K: Irreversible two-tissue compartment model; 3C5K: Irreversible three-tissue compartment model; AATH: Adiabatic Approximation to the Tissue Homogeneity; AIC: Akaike information criterion; BF: Blood flow; BIC: Bayesian information criterion; CT: Computed tomography; dPET: Dynamic PET; FDG: ^{18}F-fluorodeoxyglucose; FMISO: ^{18}F-fluoromisonidazole; IDIF: Image-derived input function; MB: Mean bias; MSEP: Mean of the squared error of prediction; NGF: Normalized gradient fields; NSCLC: Non-small cell lung cancer; pCT: Perfusion CT; PET: Positron emission tomography; RT: Radiotherapy; TACs: Time-activity-curves; VOI: Volume-of-interest

Acknowledgements

The authors would like to acknowledge the use of the University of Oxford Advanced Research Computing (ARC) facility in carrying out this work. https://doi.org/10.5281/zenodo.22558

Funding

DM is funded by a National Institute for Health Research (NIHR)/Health Education England (HEE) Clinical Lectureship (ICA-CL-2016-02-009). This paper presents independent research funded by the NIHR. The views expressed are those of the authors and not necessarily those of the NHS, the NIHR, HEE, or the Department of Health. GH is supported by a Cancer Research UK Clinician Scientist Awards (C34326/A13092 and C34326/A19590). JF was supported by a Cancer Research UK Career Development Fellowship (C17203).
The BKM120 trial is sponsored by the University of Oxford, managed by OCTRU, and supported by Cancer Research UK (C34326/A15163), the Oxford ECMC, the CRUK EPSRC Oxford Cancer Imaging Centre, the CRUK Oxford Centre, CTRad, and Novartis. The Cancer Research UK/MRC Oxford Institute for Radiation Oncology is supported by core grants from the Medical Research Council and Cancer Research UK.

Availability of data and materials

The analyzed data is available once the final trial results are published subject to reasonable request and approval by the BKM120 clinical trial office.

Authors' contributions

DM drafted the manuscript and performed data analysis. DM, MS, RM, and GH contributed to data acquisition. All authors contributed to data processing and manuscript revision. All authors read and approved the final manuscript.

Ethics approval and consent to participate

The BKM120 clinical trial (NCT02128724) has been approved by the local ethics committee (Oxford B, reference 12/SC/0674), and signed informed consent obtained from all patients.

Consent for publication

Not applicable

Competing interests

The authors declare that they have no competing interests.

Publisher's Note

Springer Nature remains neutral with regard to jurisdictional claims in published maps and institutional affiliations.

Author details
[1]Department of Oncology, University of Oxford, Oxford OX3 7DQ, UK. [2]Radiation Physics and Protection, Oxford University Hospitals NHS Foundation Trust, Oxford, UK. [3]Institute of Biomedical Engineering, Department of Engineering Science, University of Oxford, Oxford, UK. [4]Big Data Institute, Li Ka Shing Centre for Health Information and Discovery, University of Oxford, Oxford, UK. [5]Department of Radiology, Oxford University Hospitals NHS Foundation Trust, Oxford, UK. [6]School of Biomedical Engineering and Imaging Sciences, King's College London, London, UK. [7]Department of Oncology, Oxford University Hospitals NHS Foundation Trust, Oxford, UK. [8]Institute of Translational Medicine, University of Liverpool, Liverpool, UK.

Received: 23 May 2018 Accepted: 23 July 2018
Published online: 01 August 2018

References

1. Rasey JS, Koh W-J, Grierson JR, Grunbaum Z, Krohn KA. Radiolabeled fluoromisonidazole as an imaging agent for tumor hypoxia. Int J Radiat Oncol Biol Phys. 1989;17:985–91.
2. Casciari J, Graham M, Rasey J. A modeling approach for quantifying tumor hypoxia with [F-18]fluoromisonidazole PET time-activity data. Med Phys. 1995;22:1127–39.
3. Eschmann S, Paulsen F. Prognostic impact of hypoxia imaging with 18F-misonidazole PET in non-small cell lung cancer and head and neck cancer before radiotherapy. J Nucl Med. 2005;46:253–60.
4. Koh WJ, Rasey JS, Evans ML, et al. Imaging of hypoxia in human tumors with [F-18]fluoromisonidazole. Int J Radiat Oncol Biol Phys. 1992;22:199–212.
5. Thorwarth D, Eschmann S-M, Scheiderbauer J, Paulsen F, Alber M. Kinetic analysis of dynamic 18F-fluoromisonidazole PET correlates with radiation treatment outcome in head-and-neck cancer. BMC Cancer. 2005;5:152.
6. Axel L. Cerebral blood flow determination by rapid-sequence computed tomography: theoretical analysis. Radiology. 1980;137(3):679–86.
7. Grüner JM, Paamand R, Højgaard L, Law I. Brain perfusion CT compared with15O-H2O-PET in healthy subjects. EJNMMI Res. 2011;1(1):28.
8. Mullani NA, Herbst RS, O'Neil RG, Gould KL, Barron BJ, Abbruzzese JL. Tumor blood flow measured by PET dynamic imaging of first-pass F-18-FDG uptake: a comparison with O-15-labeled water-measured blood flow. J Nucl Med. 2008;49(4):517–23.
9. Fokas E, Im JH, Hill S, et al. Dual inhibition of the PI3K/mTOR pathway increases tumor radiosensitivity by normalizing tumor vasculature. Cancer Res. 2012;72:239–48.
10. McGowan DR, Macpherson RE, Hackett SL, et al. ^{18}F-fluoromisonidazole uptake in advanced stage non-small cell lung cancer: a voxel-by-voxel PET kinetics study. Med Phys. 2017;44:4665–76. https://doi.org/10.1002/mp.12416
11. van der Weerdt AP, Klein LJ, Boellaard R, Visser CA, Visser FC, Lammertsma AA. Image-derived input functions for determination of MRGlu in cardiac (18)F-FDG PET scans. J Nucl Med. 2001;42(11):1622–9.
12. Muzi M, O'Sullivan F, Mankoff DA, et al. Quantitative assessment of dynamic PET imaging data in cancer imaging. Magn Reson Imaging. 2012;30:1203–15.
13. Li F, Joergensen J, Hansen A, Kjaer A. Kinetic modeling in PET imaging of hypoxia. Am J Nucl Med Mol Imaging. 2014;4:490–506.
14. Sokoloff L, Reivich M, Kennedy C, et al. The [14C]deoxyglucose method for the measurement of local cerebral glucose utilization: theory, procedure, and normal values in the conscious and anesthetized albino rat. J Neurochem. 1977;28:897–916.
15. Bertoldo A, Peltoniemi P, Oikonen V, Knuuti J, Nuutila P, Cobelli C. Kinetic modeling of [(18)F]FDG in skeletal muscle by PET: a four-compartment five-rate-constant model. Am J Physiol Endocrinol Metab. 2001;281:E524–36.
16. Feng D, Huang SC, Wang X. Models for computer simulation studies of input functions for tracer kinetic modeling with positron emission tomography. Int J Biomed Comput. 1993;32:95–110.
17. Liu D, Chalkidou A, Landau DB, Marsden PK, Fenwick JD. 18F-FLT uptake kinetics in head and neck squamous cell carcinoma: a PET imaging study. Med Phys. 2014;41:41911.
18. Press WH, Teukolsky SA, Vetterling WT, Flannery BP. Numerical recipes in C: the art of scientific computing. 2nd ed. New York: Cambridge University Press; 1992. p. 656–706. Ch.15
19. Wald A, Wolfowitz J. On a test whether two samples are from the same population. Ann Math Stat. 1940;11:147–62.
20. Cobelli C, Foster D, Toffolo G. Tracer kinetics in biomedical research: from data to model. New York: Kluwer Academic; 2001.
21. Akaike H. A new look at the statistical model identification. Autom Control IEEE Trans. 1974;19:716–23.
22. Burnham KP. Multimodel inference: understanding AIC and BIC in model selection. Sociol Methods Res. 2004;33:261–304.
23. Picard RR, Cook RD. Cross-validation of regression models. J Am Stat Assoc. 1984;79:575–83.
24. Wang W, Georgi J-C, Nehmeh S, et al. Evaluation of a compartmental model for estimating tumor hypoxia via FMISO dynamic PET imaging. Phys Med Biol. 2009;54:3083–99.
25. Guo H, Renaut R, Chen K, Reiman E. FDG-PET parametric imaging by total variation minimization. Comput Med Imaging Graph. 2009;33:295–303.
26. Muzi M, Mankoff DA, Grierson JR, Wells JM, Vesselle H, Krohn KA. Kinetic modeling of 3′-deoxy-3′-fluorothymidine in somatic tumors: mathematical studies. J Nucl Med. 2005;46:371–80.
27. Papież BW, Heinrich MP, Fehrenbach J, Risser L, Schnabel JA. An implicit sliding-motion preserving regularisation via bilateral filtering for deformable image registration. Med Image Anal. 2014;18(8):1299–311.
28. St Lawrence KS, Lee TY. An adiabatic approximation to the tissue homogeneity model for water exchange in the brain: II. Experimental validation. J Cereb Blood Flow Metab. 1998;18:1378–85.
29. Renkin EM. Transport of potassium-42 from blood to tissue in isolated mammalian skeletal muscles. Am J Physiol. 1959;197(6):1205–10.
30. Crone C. The permeability of capillaries in various organs as determined by use of the "Indicator diffusion" method. Acta Physiol Scand. 1963;58:292–305.
31. Kelly CJ, Brady M. A model to simulate tumour oxygenation and dynamic [18F]-Fmiso PET data. Phys Med Biol. 2006;51(22):5859–73.
32. Raftery A. Bayesian model selection in social research. Sociol Methodol. 1995;25:111–63.
33. Mullani NA, Herbst RS, O'Neil RG, Gould KL, Barron BJ, Abbruzzese JL. Tumor blood flow measured by PET dynamic imaging of first-pass 18F-FDG uptake: a comparison with 15O-labeled water-measured blood flow. J Nucl Med. 2008;49(4):517–23.

Submit your manuscript to a SpringerOpen journal and benefit from:

► Convenient online submission
► Rigorous peer review
► Open access: articles freely available online
► High visibility within the field
► Retaining the copyright to your article

Submit your next manuscript at ► springeropen.com